Sustainable Food Technology

ROYAL SOCIETY OF CHEMISTRY

PAPER

View Article Online
View Journal

Cite this: DOI: 10.1039/d5fb00846h

Development and characterization of a nano-based synbiotic formulation using *Lactiplantibacillus plantarum* RJ 2 and inulin

Sangeeth S.,[a] Ananthakrishnan Jayakumaran Nair,[a] T. S. Swapna,[a] Anaswara P. A.,[bc] K. Madhavan Nampoothiri,[bc] Simi K. Varghese,[a] Suma Anish[a] and Neethu Hari *[a]

Emerging nutraceuticals aim to improve gut health by utilizing probiotics, prebiotics and synbiotics. However, the inherent instability and reduced viability of probiotics necessitate innovative nutraceutical formulations to ensure efficacy. This study reports the development of a synbiotic nano-based formulation by interacting *Lactiplantibacillus plantarum* RJ 2 with Bovine Serum Albumin (BSA) nanoparticles (BNPs) and subsequently surface functionalizing them with inulin using a sequential deposition assembly strategy. The resulting nano-based formulation functioned as an efficient synbiotic system with improved viability and structural stability. BSA nanoparticles were synthesized through a glutaraldehyde-mediated crosslinking process, yielding monodisperse particles with an average size of 59 nm. Comprehensive physicochemical characterization validated and confirmed the formation of stable BSA nanoparticles (BNPs) with well-defined spherical morphology, consistent particle size distribution, and improved colloidal stability under physiological conditions, attributed to their high negative surface charge. The inulin-functionalized probiotic-BNPs (I.BNPs) exhibited a hydrodynamic diameter of approximately 482 nm with a polydispersity index (PDI) of 0.285, confirming uniform layering and surface hydration. This synbiotic nano-based formulation demonstrated excellent physicochemical stability, high probiotic viability, and enhanced structural uniformity, as validated by different characterization techniques. Under simulated gastrointestinal (GI) conditions, this nano-based formulation achieved a 95% survival rate, demonstrating substantial enhancement in probiotic resistance to acidic and bile environments. By integrating probiotic-interacted BNPs with the prebiotic functionality of inulin, this hybrid system created a dual-acting synbiotic platform that confers both physical protection and nutritional enhancement. The developed inulin-functionalized BNP-based system represents a next-generation synbiotic formulation with potential applications in functional foods, nutraceuticals, and therapeutic probiotic delivery.

Received 31st October 2025
Accepted 2nd June 2026

DOI: 10.1039/d5fb00846h

rsc.li/susfoodtech

Sustainability spotlight

This study advances sustainable health innovation through the development of a next-generation nano-based synbiotic formulation employing biocompatible materials, including the polysaccharide inulin and bovine serum albumin (BSA)-based nanomaterial, for entrapment of probiotics and for its sustained delivery. The dual-acting platform addresses probiotic instability by combining renewable protein and prebiotic sources, ensuring high viability, structural stability, and survival under gastrointestinal stress—without reliance on synthetic additives. The approach supports greener nutraceutical systems, offering improved efficacy for gut health and enabling the integration of functional synbiotics into sustainable food and therapeutic applications, ultimately promoting resilient bioactive delivery aligned with environmentally conscious food systems.

[a]*Department of Biotechnology, University of Kerala, Kariavattom – 695 581, Thiruvananthapuram, Kerala, India. E-mail: neethuharisharon@gmail.com; dr.neethu@keralauniversity.ac.in; sanjusangeeth811@gmail.com; jekksnair@gmail.com; swapnats@yahoo.com; simivarghese1234@gmail.com; sumaanish@keralauniversity.ac.in*

[b]*Academy of Scientific and Innovative Research (AcSIR), Ghaziabad-201002, India. E-mail: anaswaraprakash001@gmail.com; madhavannampoothiri.niist@csir.res.in*

[c]*Biosciences and Bioengineering Division, CSIR – National Institute for Interdisciplinary Science and Technology (NIIST), Thiruvananthapuram – 695 019, Kerala, India*

1 Introduction

Pause for a moment to consider how much you know about the journey taken by the food you ate this morning on its way to your breakfast table. Of course, what you consume significantly affects your cognitive abilities and knowledge. Others might know very little, especially if they eat prepackaged and highly processed foods. When food is consumed in processed or

packaged forms, people typically have minimal knowledge of the larger food system, which includes the phases of food production, processing, commerce, and marketing.[1] The inherent complexity of the food system contributes to contamination risks and food-borne disease, creating a growing demand for nutraceutical approaches that promote gut health through probiotics, prebiotics, and synbiotics. However, the inherent instability and reduced viability of probiotics necessitate innovative nutraceutical formulations to ensure efficacy. Probiotics are specifically defined as viable, non-pathogenic microorganisms that confer a health benefit on the host when administered in adequate amounts,[2] thereby conferring a promising approach to combat food-borne diseases by reducing the pathogenic potential of harmful microorganisms.[3]

Probiotic bacteria, primarily belonging to the genera *Lactobacillus* and *Bifidobacterium*,[2] provide numerous benefits to the host organism. Colonization by these beneficial microorganisms facilitates the elimination of pathogens, enhances resistance to subsequent colonization, and results in the production of vitamins, bacteriocins, and immunomodulatory compounds that modulate the host immune response.[4] To confer their beneficial effects, probiotics must possess specific functional properties, including tolerance to the harsh conditions of the gastric environment, metabolic activation, and targeted delivery to the lower gastrointestinal tract in sufficient quantities.[5,6]

Prebiotics are non-digestible food components, especially dietary fibres such as inulin and fructo-oligosaccharides, which are resistant to gastric acidity and small intestine enzymes, promoting the growth and activity of beneficial bacteria in the gut by delivering fermentable carbohydrates to probiotics in the colon.[7] Inulin supplementation has been shown to mitigate the detrimental effect of high-fat diets on the mucus layer's permeability and metabolic processes.[8–10] The intestine is the primary target for both probiotics and prebiotics[11] and the combination of these two components, known as "synbiotics," exhibits synergistic properties and has been shown to increase the viable counts of *Lactobacilli* and *Bifidobacteria* compared to the use of probiotics or prebiotics alone.[12] In synbiotic formulations, the prebiotic component serves as a protective agent, protecting the probiotic from stomach acidity and enzymatic degradation. Therefore, careful selection of the combination of prebiotics and probiotic microorganisms is crucial to maximize the benefits of synbiotics over the use ofprobiotics or prebiotics alone.[13]

Since probiotics are typically administered orally, they are often inactivated by the harsh gastrointestinal (GI) environment. However, recent research reveals that nanoencapsulation offers a promising approach to safeguard probiotics during processing and gastrointestinal transit, ensuring their viability and efficacy.[14,15] BNPs are biocompatible, non-toxic protein-based nanomaterials with high binding affinity for pharmaceuticals and bioactive molecules. Consequently, BNPs has explored applications in drug administration, diagnostic imaging, and therapeutics.[16] The Layer-by-Layer (LbL) method is a widely used sequential deposition strategy for encapsulating probiotics, enabling the sequential deposition of cationic (*e.g.*, chitosan) and anionic (*e.g.*, gellan gum) polymer layers onto the bacterial surface through electrostatic interactions.[17,18] The LbL technique confers probiotic stability by rendering resistance to acidic conditions and bile salts, thereby facilitating their growth in targeted areas of the intestinal region.[17–19] Recently, Liu *et al.* (2023) reported the effectiveness of LbL self-assembly using zein nanoparticles and pectin, which imparts enhanced *Lactobacillus plantarum 550* survival under harsh gastrointestinal (GI) circumstances.[20] The present work focuses on the development of a stable nano-based synbiotic system by entrapping a probiotic organism (*Lactiplantibacillus plantarum* RJ 2) with BNPs, followed by a sequential layer of prebiotic inulin by a sequential deposition method and their characterization. Unlike conventional polysaccharide carriers such as alginate and chitosan, BNPs offer higher structural stability, tunable surface functionality, and superior compatibility with bioactive molecules. These characteristics make them suitable for the synthesis of a stable nanosynbiotic system, resistant to several environmental stresses, including temperature, pH, various gases, water, and moisture. Such a nanosynbiotic system confers enhanced stability for probiotics and improved nutritional aspects and is endowed with controlled release characteristics. This may lead to the production of high-quality nano-synbiotic-based food items with improved bioavailability. In this respect, the current study looks into surface functionalized BNPs as a nanoentrapment platform for improving the stability, protection, and enhanced efficacy of synbiotic formulations, presenting a promising alternative to standard nano-carrier systems.

2 Materials and methods

2.1. Materials and chemicals

Lactiplantibacillus plantarum RJ 2 was previously isolated from a rotten jackfruit. de Man, Rogosa, and Sharpe (MRS) broth, bovine serum albumin (BSA), sodium chloride (extra pure), bile salts (microbiological grade), and antibiotic discs (Hexa G-Minus 8) were procured from HiMedia Laboratories Pvt. Ltd (Mumbai, India). Folin reagent and inulin (extra pure) were obtained from Sigma-Aldrich (St. Louis, MO, USA).

2.2. Preparation of *Lactiplantibacillus plantarum* RJ 2

Lactiplantibacillus plantarum RJ 2 was grown in MRS broth at 37 °C ± 2 °C under optimal incubation conditions, such as an aerobic environment and an incubation period of 18–24 hours until the cells reached the logarithmic growth phase. After cultivation, the bacterial cells were harvested by centrifugation at 4000 rpm for 10 min at 4 °C and used for surface coating procedures. Viable cells were quantified using the conventional plate count technique, with each plate containing 30 to 300 colonies. The colony-forming unit (CFU) was calculated as the average of three independent measurements, and the final CFU values were calculated for 1 mL of solid material.[20]

2.3. Synthesis of bovine serum albumin nanoparticles (BNPs)

BNPs were synthesized *via* a modified desolvation method.[21] Briefly, 100 mg of BSA was dissolved in 5 mL of deionized water and subjected to mechanical stirring (500 rpm) for 10 min at 25 ± 2 °C. Subsequently, 20 mL of absolute ethanol was added dropwise to induce nanoparticle formation, resulting in an amber-coloured suspension. After a 5-minute incubation, 8% (v/v) glutaraldehyde was added to cross-link the BNPs. The mixture was then subjected to magnetic stirring for 24 h at room temperature (30 ± 2 °C). The resulting suspension was centrifuged thrice at 9000 rpm for 10 min each, with intermediate resuspension in 10 mL deionized water. The purified nanoparticles were dried at room temperature (30 ± 2 °C) and stored at 4 °C for further analysis.

2.4. Structural characterization of BNPs

BNPs were characterized using various analytical methods, including UV-Vis spectroscopy, FTIR, XRD, FE-SEM, DLS, and zeta potential. The absorption spectra of BNPs were recorded using a UV spectrophotometer (Agilent Technologies Cary 5000), while FTIR spectroscopy (ThermoScientific Nicolet iS50) was employed to identify specific functional groups and validate nanoparticle production and cross-linking. XRD analysis (Bruker D8 ADVANCE with DAVINCI design) was performed to determine the crystallinity of BNPs, with diffraction patterns recorded over a 2θ range of 10 °C – 80 °C. FE-SEM (Nova NanoSEM 450, UoK) was used to assess surface morphology, size distribution, and surface characteristics. Finally, zeta potential and DLS measurements were performed using a Horiba SZ100 DLS system to evaluate nanoparticle stability and size distribution (hydrodynamic size), respectively. About 250 μL of the synthesized BNPs were dispersed in Milli-Q water, making a final volume of 4 mL, and then the colloidal solution was sonicated for 15 minutes. The well-dispersed colloidal solutions were investigated for particle size, polydispersity index (PDI) and zeta potential.

2.5. Estimation of BNPs by Folin–Lowry's method

The Folin–Lowry method was employed to quantify the protein content of BNPs and assess the retention of BSA's native properties after nanoparticle formation. Briefly, BNPs with varying concentrations (6.25 μg mL^{-1}, 12 μg mL^{-1}, 25 μg mL^{-1}, 50 μg mL^{-1} and 100 μg mL^{-1}) were treated with an alkaline copper reagent and incubated for 10 minutes, followed by treatment with the Folin reagent. Then the reaction mixture was subjected to a 30-minute incubation in the dark at room temperature (30 ± 2 °C). After the incubation, the absorbance was measured at 660 nm. Protein content was calculated using a standard curve generated with 1 mg mL^{-1} BSA, with triplicate measurements ensuring precision and accuracy.

2.6. Preparation and characterization of *Lactiplantibacillus plantarum* RJ 2 and I.BNPs

2.6.1 Preparation of *Lactiplantibacillus plantarum* RJ 2-loaded synbiotic nanoformulation. For entrapment, initially, BNPs and inulin stock solutions were prepared at a concentration of 2 mg mL^{-1} in deionized water. Then, 2 mL of bacterial suspension (*Lactiplantibacillus plantarum* RJ 2) was mixed with 8 mL of BNPs for 15 minutes at room temperature (30 ± 2 °C), followed by the addition of 10 mL of inulin solution under constant stirring at 500 rpm at room temperature (30 ± 2 °C). After 15 minutes, the mixture was centrifuged at 10 000 rpm for 10 minutes and washed twice with deionized water to remove excess BNPs and inulin solution. The resulting sample was named I.BNPs. These nanoformulations were stored at 4 °C for further experiments.[20]

2.6.2 Determination of bacterial viability and growth. For evaluating the cell viability of the probiotic and I.BNPs, the samples were serially diluted in 0.85% saline. Following dilution (10^{-3} and 10^{-5}), 0.1 mL of each sample was spread-plated on MRS agar and incubated at 37 °C for 24 hours. Colony enumeration was carried out in triplicate, and plates with 200–350 colonies were considered for counting. The results were expressed in colony-forming units (CFU) per mL of solution with a modified procedure.[22]

2.6.3 Acid tolerance. The acid tolerance of *Lactiplantibacillus plantarum* RJ 2 (10^8 CFU mL^{-1}) and the I.BNPs were evaluated by inoculating 100 μL of an overnight-grown culture into 10 mL of MRS broth adjusted to pH 2.5 and 1.5 using 1 M HCl, following a modified version of the method described by Fang *et al.* and mixed thoroughly.[23] The samples were then incubated at 37 °C for 3 hours. Following incubation, the amount of viable cells was determined by plating on MRS agar plates. Survival rates were computed with the following equation:

$$\text{Survival rate (\%)} = (C_1/C_0) \times 100$$

where C_1 is the number of cells after acid treatment and C_0 is the initial cell count. The results were presented as colony-forming units (CFU) per mL. Survival rates were recorded at different acidity levels to assess the ability of both formulations to withstand harsh gastric conditions, and the above tests were carried out in triplicate.

2.6.4 Bile salt resistance. Bile salt tolerance of *Lactiplantibacillus plantarum* RJ 2 and I.BNPs was evaluated by assessing their survival in MRS broth prepared with and without 0.3% bile salts, and both media were inoculated with 1% of the bacterial culture. The bile salt resistance of *Lactiplantibacillus plantarum* RJ 2 and I.BNPs was evaluated at different time intervals using the spread plate method and the cultures were grown at 37 °C, and viable cell counts were measured at 4, 5, and 6 hours after inoculation followed by the spread plate method following a 5-fold serial dilution; specifically, 10^{-3} and 10^{-5} diluted samples were plated (0.1 mL each) on MRS agar, incubated at 37 °C for 24 hours, and enumerated to determine bacterial viability[24] and the experiment was carried out in triplicate. The growth rate in

bile salt-containing media was expressed as a percentage compared to the control using the following equation:

$$\% \text{ of Growth} = (\text{Growth in the bile salt medium}/\text{Growth in the control medium}) \times 100$$

2.6.5 Antibiotic resistance profiling of *Lactiplantibacillus plantarum* RJ 2 and I.BNPs using the disc diffusion assay. The antibiotic resistance profile of *Lactiplantibacillus plantarum* RJ 2 and I.BNPs was evaluated using the disc diffusion assay. Bacterial suspensions were prepared and uniformly spread on MRS agar plates. Antibiotic discs containing amikacin (30 mcg), ceftazidime (30 mcg), aztreonam (30 mcg), piperacillin (100 mcg), imipenem (10 mcg), and ciprofloxacin (5 mcg) were aseptically applied to the agar surface. Plates were incubated at 37 °C for 24 hours. Following incubation, the diameters of inhibition zones were measured and analyzed to determine the antibiotic susceptibility patterns.

2.6.6 Auto-aggregation and co-aggregation ability. The auto-aggregation ability of *Lactiplantibacillus plantarum* RJ 2 and I.BNPs was tested after 24 hours of incubation in MRS broth at 37 °C under microaerophilic conditions (2–10% O_2). Probiotic culture was harvested by centrifugation at 4000 rpm for 10 minutes, then washed, and resuspended in 10 mL of PBS to achieve a final concentration of approximately 10^8 CFU mL^{-1} (OD_{550} 0.2–0.3). The suspensions were vortexed for 10 seconds and then incubated at room temperature (30 ± 2 °C) for 6 hours. At hourly intervals, 1 mL of the upper phase was collected, and the absorbance at 600 nm was determined. The proportion of auto-aggregation was computed using the equation below:

$$\text{Auto-aggregation}(\%) = [(A_x - A_y)/A_x] \times 100$$

where A_x is the absorbance at time $(t) = 0$ and A_y is the absorbance at different time points.

The co-aggregation ability was assessed for the free probiotic cells and for encapsulated cells by combining 2 mL aliquots of probiotic cells and two enteropathogenic bacteria (*E. coli* MTCC 40 and *Staphylococcus aureus* ATCC 25923) suspensions and vortexing for 10 seconds. All suspensions were incubated at room temperature (30 ± 2 °C) for six hours. At hourly intervals, 1 mL of the upper phase was collected, and absorbance was determined at 600 nm. The proportion of co-aggregation was computed using the formula below:

$$\text{Co-aggregation}\ (\%) = \{[(A_{\text{pro}} + A_{\text{pat}}) - A_{\text{mix}}]/(A_{\text{pro}} + A_{\text{pat}})\} \times 100$$

where $A_{\text{pro}} + A_{\text{pat}}$ represents the individual aggregation properties of *Lactiplantibacillus plantarum* RJ 2 and the pathogen at time 0 h and A_{mix} denotes their combined aggregation at different time points. All experiments were conducted in triplicate to ensure reproducibility.[25]

2.7. Structural characterization of I.BNPs

I.BNPs were characterized using various analytical techniques, including FTIR, XRD, DLS, and zeta potential. FTIR spectroscopy (Thermo Scientific Nicolet iS50) was used to detect and validate certain functional groups in inulin and I.BNPs. XRD analysis (Bruker D8 ADVANCE with DAVINCI design) was conducted to determine the crystalline nature of I.BNPs and inulin. Diffraction patterns were acquired across a 2θ range of 10°–80°. The microorganism's surface shape, size distribution, and surface properties were evaluated using FE-SEM (ZEISS FESEM). Finally, DLS and zeta potential measurements were performed with a Horiba SZ100 DLS device to assess entrapment reliability and size distribution (hydrodynamic size).

2.8. Statistical analysis

All the experiments were performed in triplicate ($n = 3$ independent experiments), and the results were represented as mean ± SD. Using GraphPad Prism software (Version 8.0), statistical analysis was performed. The Student's *t*-test was used to assess statistical differences between two experimental groups. Statistical significance was denoted as p-value ≤ 0.05, with significance levels mentioned as $*p < 0.05$, $**p < 0.01$, $***p < 0.001$ & $****p < 0.0001$.

3 Results and discussion

3.1. Synthesis of BSA nanoparticles

BNPs with a nearly spherical morphology are produced using the desolvation method, as verified through various structural characterization approaches. In this process, the incorporation of glutaraldehyde as a crosslinking agent enhances nanoparticle stability by forming Schiff base linkages. These bonds arise from the reaction between the aldehyde groups (–CHO) of glutaraldehyde and the primary amine groups ($–NH_2$) present in lysine (ε-amino) and arginine (guanidinium) residues on the BSA surface. The resulting covalent imine bonds (–CH═N–R) establish a three-dimensional crosslinked protein matrix, which inhibits redissolution while preserving the integrity of the hydrophobic core.[26]

3.2. Structural characterization of BNPs

The UV spectrum reveals a distinct redshift in the primary absorbance peak, shifting from 278 nm in native BSA to 289 nm in BNPs (SI Fig. 1). This shift suggests the successful transformation of the protein into nanoparticle form. Additionally, the change in peak intensity along with the slight shift in wavelength (278 nm to 289 nm) indicates conformational alternation.

The broader and slightly lower-intensity BNP peak suggests partial unfolding or exposure of aromatic rings of amino acid residues such as tryptophan, tyrosine, and phenylalanine, while the retained absorbance confirms that the protein backbone remained intact. Consistent with previous findings, UV-Vis spectra of BNPs revealed structural changes during nanoparticle formation, including side chain modification and backbone environments. Specifically, the primary backbone absorption band (~192 nm) experiences reduced intensity and peak shift due to glutaraldehyde crosslinking. The aromatic residue-associated peak (~278 nm) is relatively preserved with

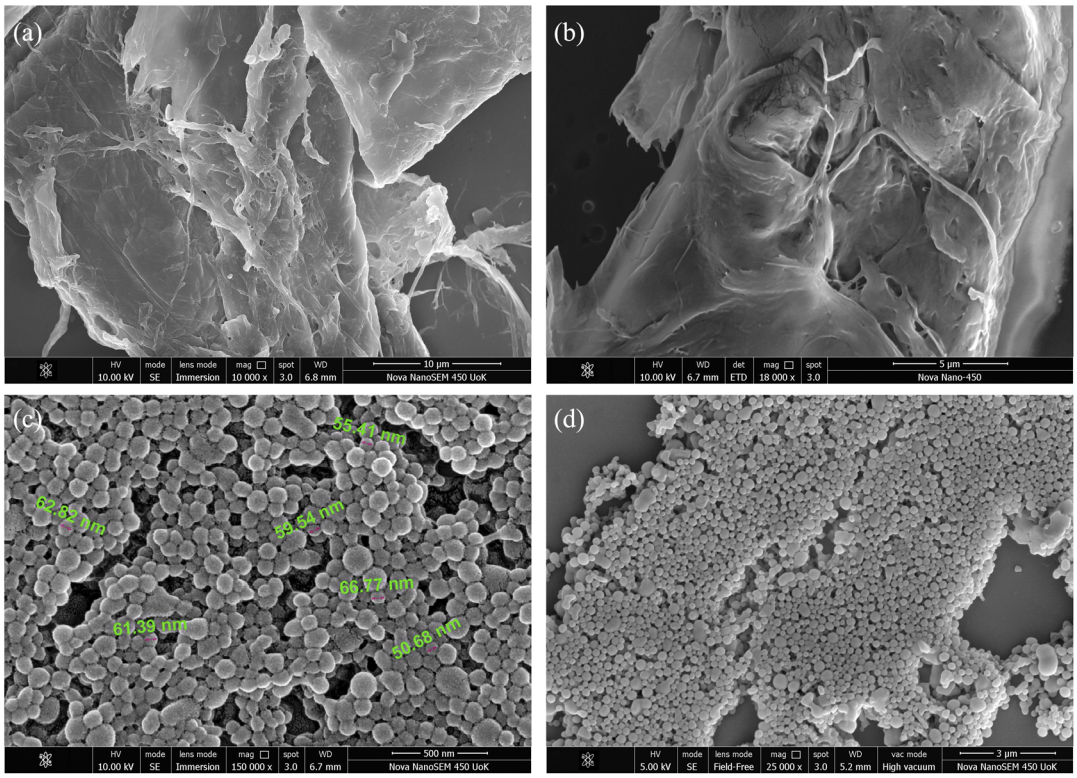

Fig. 1 Scanning electron microscopy (SEM) images of (a and b) BSA, (c and d) BNPs at 10 000 ×, 18, 000 ×, 150 000 × and 250 00×, respectively.

minor alteration, indicating the retention of functional groups responsible for ligand binding.[21] Retained aromatic absorbance ensures the preservation of major residues, supporting successful nanoparticle formation with a modified tertiary structure and intact protein integrity. The broadened and lower-intensity profile of BNPs reflects partial unfolding and structural rearrangement without complete denaturation.

The FE-SEM analysis of BNPs, shown in Fig. 1(c and d), reveals a densely packed arrangement of nanoparticles with a size range of approximately 59.43 nm ± 5.2 nm with almost consistent size and spherical morphology, evidencing successful and reproducible nanoparticle synthesis. In comparison, FE-SEM imaging of bulk BSA in Fig. 1(a and b) demonstrates an irregular, coarse morphology. The smooth and spherical morphology of BNPs observed here is advantageous for various biological applications by reducing non-specific interactions and enhancing circulation stability,[16] and these morphological features align with recent reports demonstrating similar nanoparticle characteristics and their functional benefits, confirming efficient nanoparticle fabrication and clear structural differentiation from bulk BSA. The magnitude value of zeta potential measurements confirms a significant increase in absolute surface charge from BSA (24 mV) to BNPs (32.3 mV), indicative of enhanced electrostatic repulsion and colloidal stability. This higher magnitude of zeta potential for BNPs minimizes aggregation propensity,[26] a critical factor ensuring stable dispersion for nano-based biological applications. Dynamic light scattering (DLS) analysis determined the hydrodynamic diameter of BNPs to be 28.5 ± 1.2 nm with PDI 0.124 ± 0.03 ($n = 3$) (Fig. 2). This size represents the DLS-derived z-average hydrodynamic diameter, which corresponds to the effective particle size in dispersion rather than the dry core diameter. The low PDI (<0.2) confirms a monodisperse nanoparticle population with narrow size distribution and excellent colloidal stability with minimal aggregation and high uniformity,[27] confirming their nanoscale dimension and suitability for biomedical applications.[16] Such nanoscale dimensions are consistent with the reported behaviour of BSA-based nanoparticle systems and are appropriate for subsequent surface functionalization and probiotic entrapment.[28] In the FTIR spectra (Fig. 3) of BNPs, the prominent absorbance peaks at 1632 cm^{-1} (amide I; C═O stretching) and 1532 cm^{-1} (amide II;

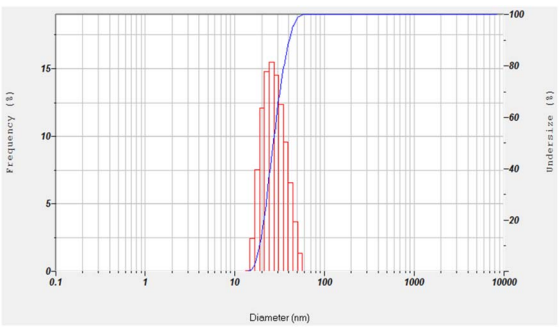

Fig. 2 Hydrodynamic size of BNPs.

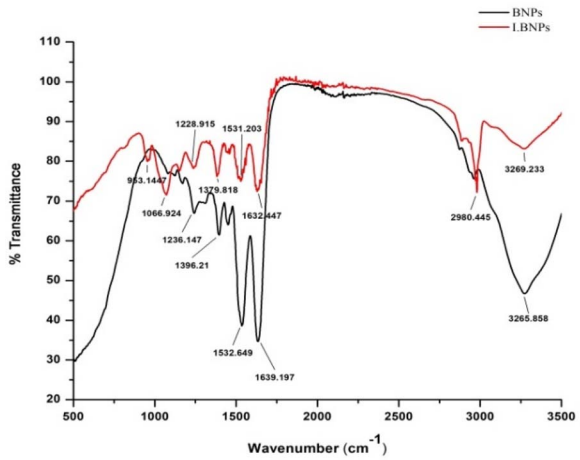

Fig. 3 FTIR spectra of BNPs and I.BNPs.

N–H bending and C–N stretching) represent the secondary structure of proteins. The strong broad band at 3265 cm^{-1}, which exhibits intermolecular hydrogen bonding between polypeptide chains, is attributed to O–H and N–H stretching. Minor bands at 1236 and 1396 cm^{-1} are linked to C–N stretching and CH_2 bending, while peaks between 953 and 1066 cm^{-1} are created by C–O stretching and protein skeletal vibrations. These spectrum designations are consistent with well-structured, native BSA (SI Fig. 2) and confirm that the amide environments and protein backbone are maintained during nanoparticle formation. These data further support previous studies indicating that amide I and II bands serve as dependable indicators of the structural integrity of BNPs.[16]

An amorphous nanostructured protein matrix is characterized by a broad peak found at 20–30° 2θ in the XRD profile of BNPs in Fig. 4. The lack of distinct, crisp crystalline reflections reveals that the generated BNPs are structurally disordered and lack long-range order, which is a characteristic of biomolecular systems made by crosslinking or nanoprecipitation techniques. However, a distinct, crystalline characteristic peak was observed in BSA (SI Fig. 3), indicating the presence of ordered structural domains. In light of recent studies,[29,30] which reported similar features for pure BSA and BNPs, such a broad pattern in XRD is a standard indication of amorphous albumin-based materials. In line with contemporary protein-based nanosystem applications, this amorphous structure can improve entrapment and release characteristics.

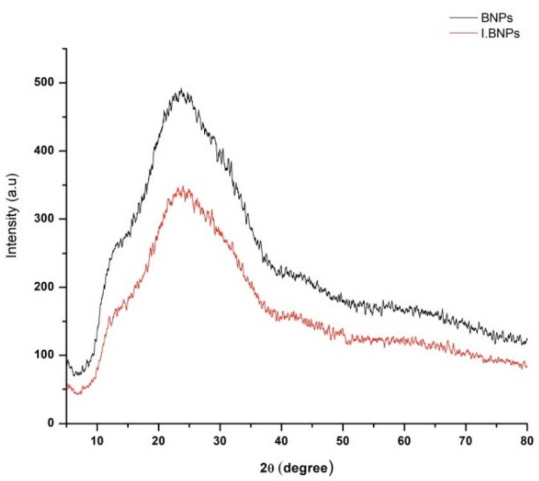

Fig. 4 XRD spectra of BNPs and I.BNPs.

3.3. Estimation of BNPs by Folin–Lowry's method

Protein estimation using the Lowry method was performed as described in the methodology section, confirming the protein nature of BNPs at an absorbance of 660 nm. The activity of nanoparticle concentrations was determined as detailed in the methodology and is presented in Table 1 (SI). A linear relationship was observed, with absorbance increasing proportionally with concentration, indicating a direct correlation (Fig. 5). These results confirm that the protein characteristics and structural stability of BSA were preserved even at the nanoscale during nanoparticle formulation.[31] Separate graphs illustrate the standard curve (SI Fig. 4) and corresponding nanoparticle concentrations.

3.4. Microbial characterization of *Lactiplantibacillus plantarum* RJ 2 and nano-based synbiotic formulation

3.4.1 Bacterial enumeration assay. The cell viability of *Lactiplantibacillus plantarum* RJ 2 and I.BNPs demonstrated that probiotic release from the synbiotic nanoformulation exhibited enhanced viability compared to the free cells. At the 10^{-3} dilution, CFU counts were 8.62×10^6 CFU mL^{-1} for the encapsulated cells *versus* 8.05×10^6 CFU mL^{-1} for free cells. Similarly, at the 10^{-5} dilution, encapsulated cells retained 8×10^5 CFU mL^{-1} compared to 3.2×10^5 CFU mL^{-1} for free cells, indicating improved probiotic survival due to entrapment. These findings

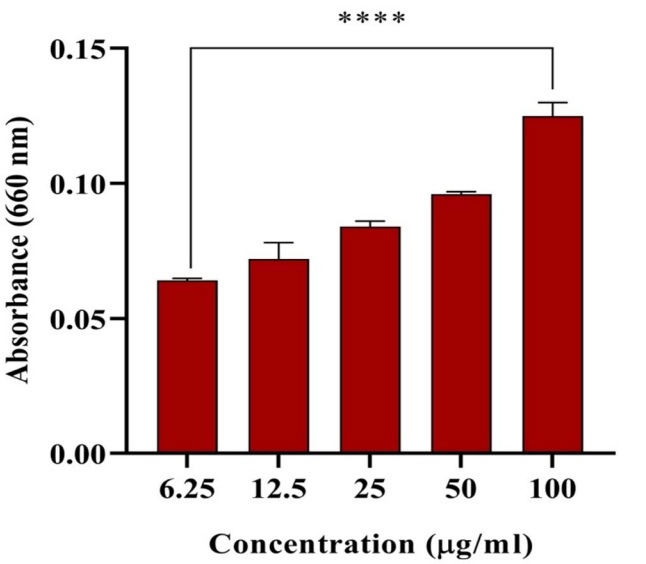

Fig. 5 The protein quantification of BNPs using the Lowry method. Data are represented as mean ± SD with statistical significance between 6.25 µg mL^{-1} and 100 µg mL^{-1} ($p < 0.0001$).

correlate with previous reports where protein-based nanoparticle entrapment, such as with whey and zein proteins, provided excellent probiotic viability, showing low log reductions and maintaining viable counts near 10^7 CFU g^{-1} and 10^6 CFU g^{-1}, respectively.[32] This evaluation indicates that the interaction of BNPs with probiotics influences their viability.

3.4.2 Acid tolerance. Under highly acidic conditions (pH 2.5), *Lactiplantibacillus plantarum* RJ 2 and I.BNPs exhibited similar survival rates of 57.91% and 57.95%, respectively. While free cultures lost viability completely at pH 1.5, the synbiotic formulation retained 13.5% survival, indicating that BSA and inulin matrices provided substantial acid protection, and upon entrapment, the organism can survive under the acidic conditions, and its sustained release (for $\approx$ 3 h) is maintained over that environment. The gastric environment typically exhibits a pH range of 1.5–4.5, with an average gastric residence time. Acid tolerance is a critical characteristic required for probiotic microorganisms to withstand the harsh gastric conditions and retain their viability during transit through the stomach. A study conducted by Bhagawat *et al.* (2020)[33] showed comparable acid defence properties where *Enterococcus* cells exhibited improved survival rates upon entrapment in maltodextrin-based spray-dried microcapsules at pH 2.0–2.5. Sakoui *et al.*[34] demonstrated that the probiotic encapsulation in inulin–maltodextrin–sodium alginate matrices significantly enhances probiotic viability (>85% viability) in simulated gastric fluid. A recent report revealed that the *L. plantarum* encapsulated in a nanocellulose hydrogel retained >8 log CFU g^{-1} under simulated gastric conditions, confirming the efficient stabilization of probiotics under acid stress.[35]

3.4.3 Bile salt resistance. The bile salt tolerance assay revealed that I.BNPs substantially enhanced the survival and growth of *Lactiplantibacillus plantarum* RJ 2 under simulated gastrointestinal stress. At the 10^{-3} dilution, free cells exhibited 88.75%, 92.57%, and 95.92% growth in the 4th, 5th, and 6th hours, respectively, whereas I.BNPs showed a slightly higher growth of 92.3%, 95.38%, and 98.3% at the corresponding time points. At the 10^{-5} dilution, *Lactiplantibacillus plantarum* RJ 2 demonstrated 14.81%, 29.75%, and 61.36% growth in the 4th, 5th, and 6th hours, respectively, while I.BNPs exhibited significantly enhanced growth of 21.21%, 49.12%, and 74.6% over the same period. These findings suggest that the nanoparticle matrix mitigates bile-induced cell membrane disruption, thereby promoting sustained bacterial proliferation during extended bile exposure. Comparable enhancements in bile salt resistance were documented by Xin *et al.* (2025)[36] where *L. plantarum* encapsulated within sodium alginate–pectin–polyphenol matrices exhibited improved tolerance against bile stress. Mechanistically, the bile salt hydrolase (BSH) system plays a central role in *L. plantarum* adaptation, facilitating deconjugation of bile acids into less toxic derivatives that support membrane stability.[37] Furthermore, inulin-based encapsulation provides additional protection through prebiotic support and membrane reinforcement, improving survival efficiency under bile-mediated oxidative stress.[38]

3.4.4 Antibiotic resistance characteristics of *Lactiplantibacillus plantarum* RJ 2 and I.BNPs against various antibiotics. The disc diffusion assay revealed that both *Lactiplantibacillus plantarum* RJ 2 and I.BNPs exhibited pronounced resistance to all tested antibiotics (SI Fig. 5a & b), suggesting the presence of intrinsic, non-transferable resistance mechanisms. This observation aligns with recent findings, where *L. plantarum* strains displayed strain-dependent antibiotic resilience associated with chromosomal efflux systems and cell wall impermeability.[39,40] Sarangarajan *et al.*[41] proved that prebiotic-based synbiotic administration reduces antibiotic-induced gut dysbiosis and downregulates resistance gene expression. Likewise, inulin-driven encapsulation systems have been shown to stabilize probiotic viability while preventing horizontal gene transfer.[42]

These findings confirm that *Lactiplantibacillus plantarum* attains intrinsic resistance by synbiotic formulations and can mitigate the impact of antibiotics while retaining probiotic functionality.

3.4.5 Auto-aggregation and co-aggregation ability. The results of auto-aggregation and co-aggregation analyses for *Lactiplantibacillus plantaraum* RJ 2 and I.BNPs are presented in Fig. 6. Both strains exhibited notable auto-aggregation capabilities, with aggregation percentages progressively increasing over the incubation period ($p < 0.001$) Fig. 6(a and b). The I.BNPs displayed the highest aggregation, reaching $94.4 \pm 0.63\%$ in the 6th hour, indicating that entrapment enhanced intercellular adhesion and stability. This time-dependent rise in aggregation suggests that surface-associated components such as proteinaceous adhesins, exopolysaccharides (EPSs), and polysaccharide protein complexes play a critical role in facilitating cell–cell interactions. Comparable findings have been reported in the literature, where upon 5 h of incubation, certain *Lactobacillus gasseri* and *L. crispatus* strains exhibited auto-aggregation levels exceeding 90%, while the *Lactobacillus rhamnosus* GG control achieved only 23% at the same time point.[43] Similarly, Isenring *et al.*[44] demonstrated that *L. plantarum* gradually increases its auto-aggregation over extended incubation times, a behaviour linked to biofilm establishment and intestinal colonization potential. Zawistowska-Rojek *et al.*[45] emphasized that aggregation behaviours in Lactobacillaceae are strain-dependent and correlate strongly with probiotic adhesion efficiency and pathogen exclusion capacity. These observations affirm that the enhanced auto-aggregation observed in I.BNPs supports improved adhesion competence and biofilm-forming potential, a crucial trait for gut persistence and colonization.

Co-aggregation assays with two indicator pathogens revealed that all tested probiotic strains demonstrated measurable aggregation with the pathogenic cells ($p < 0.01$) Fig. 6(c and d). However, the degree of co-aggregation was distinct across strains and varied with incubation time, confirming its strain-specific and time-dependent nature. The I.BNPs exhibited the highest co-aggregation with enteropathogenic *Escherichia coli* MTCC 40 and *Staphylococcus aureus* ATCC 25923, signifying that nanoparticle entrapment enhances surface-mediated adherence and interspecies cellular interactions. Such behaviour is vital for the competitive exclusion of pathogens within the gastrointestinal tract. These findings are consistent with observations by Klopper *et al.*,[46] who demonstrated that the aggregation capacity of Lactobacillaceae allows them to form

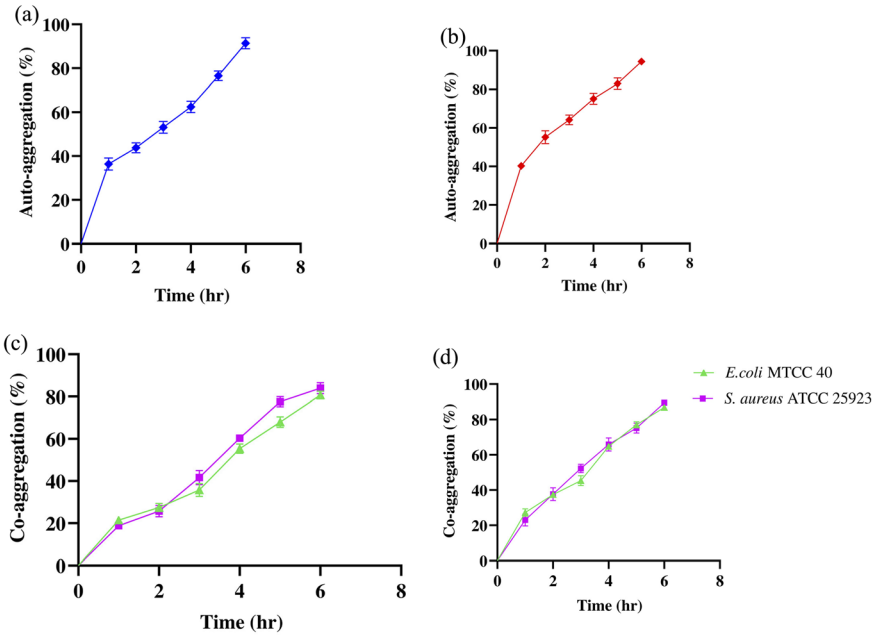

Fig. 6 (a and b) The auto-aggegation percentage of *Lactiplantibacillus plantarum* RJ 2 and I.BNPs and (c and d) the co-aggregation percentage with enteropathogenic *Escherichia coli* MTCC 40 and *Staphylococcus aureus* ATCC 25923 by *Lactiplantibacillus plantarum* RJ 2 and I.BNPs. Values are presented as mean ± standard deviations.

physical barriers, minimizing pathogen attachment to gut epithelial receptors. Sophatha *et al.*[47] reported that *Lactobacillus* strains exhibited co-aggregation percentages ranging from 21% to 66% with enterotoxigenic pathogens such as *E. coli* and *S. enterica*, depending on incubation duration and strain specificity. Importantly, they noted a positive correlation between auto-aggregation capacity and subsequent co-aggregation performance. Zawistowska-Rojek *et al.*[45] also established the interdependent properties of co-aggregation and auto-aggregation, crucial for adhesion, pathogen interference, and the maintenance of beneficial microbial populations in the gut ecosystem.

3.5. Structural characterization of I.BNPs

During the sequential deposition assembly process, the zeta potential reversed sequentially with each deposited layer, reflecting the alternate electrostatic adsorption of oppositely charged biomolecules. The I.BNPs exhibited a net magnitude of 20 mV, confirming the successful formation of a multilayer nano-based formulation with stable electrostatic interactions. The observed "zig-zag" variation in zeta potential across the successive layers verified the ordered deposition of alternating charges, characteristic of well-defined sequentially deposited assemblies. Similar trends of zeta-potential inversion during multilayer electrostatic deposition have been reported for probiotic and biopolymer-based nanodelivery systems.[48,49] The final negatively charged surface obtained for the I.BNPs comparable to that of previously described inulin and protein-based nanoparticle formulations[50] is expected to enhance their electrostatic attraction toward positively charged mucosal surfaces, thereby facilitating improved intestinal adherence, retention, and targeted probiotic delivery efficiency.

The hydrodynamic diameter of I.BNPs was determined to be 482.7 ± 12.4 nm using dynamic light scattering (DLS), with PDI = 0.285 ± 0.04 (n = 3) (Fig. 7). PDI < 0.3 confirms narrow size distribution and good colloidal stability of multilayered nanostructures. The single intensity peak at ~483 nm indicates uniform inulin-BSA assembly with controlled hydration shell formation, indicating the formation of hydrated, multilayered nanostructures arising from sequential inulin and BNP assembly.[51] This nanoscale dimension verifies the successful fabrication of stable, polydisperse nanoparticles suitable for probiotic delivery applications. An increase in size relative to bare BNPs was observed, consistent with reports that polysaccharide–protein hybrid coatings contribute to larger hydrodynamic diameters through hydration shell formation and charge-induced aggregation control.[52,53] DLS analysis, based on Brownian motion and scattering fluctuation measurements, provides a non-invasive method to assess particle diffusion behaviour in suspension.[54] The measured particle size encompasses both the nanoparticle core and its associated solvation layer.[16]

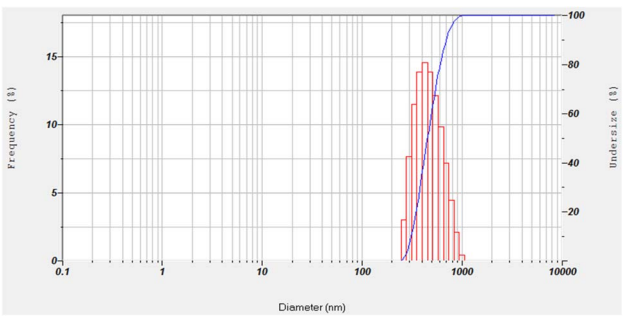

Fig. 7 Hydrodynamic size of I.BNPs.

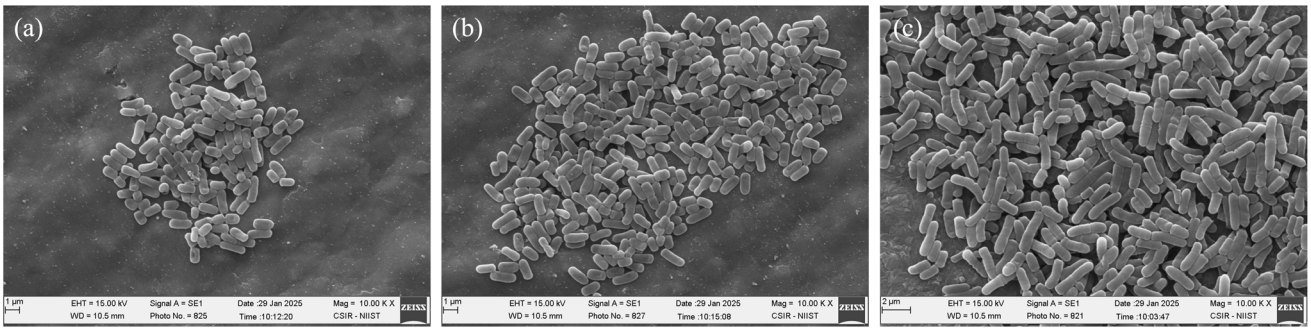

Fig. 8 FE-SEM image of (a and b) *Lactiplantibacillus plantarum* RJ 2 and (c) surface coated *Lactiplantibacillus plantarum* RJ 2 at 10.00K×.

FESEM micrographs revealed distinct morphological differences between the free *Lactiplantibacillus plantarum* RJ 2 cells and the I.BNPs. Fig. 8(a and b) shows free bacterial cells displaying a uniform rod-shaped morphology with smooth surfaces, homogeneous dimensions, and dense spatial distribution, indicating healthy cell organization. In contrast, Fig. 8(c) illustrates the surface-coated cells arranged as relatively loose clusters with occasional filamentous extensions at the cell periphery. These observed filamentous structures likely result from partial deposition of inulin–BSA components during layer-by-layer coating, which alters cell surface charge distribution and weakly affects division symmetry.

The filamentous cell pattern could also indicate a mild physiological stress response caused by the nanoparticle interaction or surface deposition effect. Similar filamentation phenomena in *L. plantarum* under environmental or physicochemical stress (acidic, oxidative, or coating-induced) have been associated with transient inhibition of cell division or peptidoglycan remodelling processes, resulting in elongated or chained morphotypes.[55,56] These changes are generally adaptive rather than deleterious, facilitating temporary resistance against surface tension and oxidative stress.[55] Despite minor morphological alterations, the overall cellular integrity exhibits an intact nature with smooth, continuous membrane surfaces and no evidence of rupture or deformation. This preservation of structure indicates that the coating did not compromise cell viability.[57,58] The surface modifications observed here likely represent physiological adaptation rather than cell injury, corroborating the high viability and functional stability measured in corresponding survival assays.

A broad, low-intensity peak in the XRD spectrum of I.BNPs (Fig. 5) is observed, which is consistent with an amorphous morphology and the lack of long-range crystalline organization. The integration of the inulin polysaccharide on the nanoparticle surface is responsible for the enhanced structural disorder as evidenced by the decreased peak intensity and loss of unique reflections as compared to raw BNPs. The amorphous nature of the inulin (SI Fig 6) is retained in the I.BNPs after the surface functionalization. According to recent studies[59,60] this broad halo pattern corresponds to standard XRD signatures of an amorphous protein–polysaccharide nanomaterial, and the studies emphasize these features as indicators for the homogeneous, non-crystalline assembly in functional biopolymer nanocarriers. These spectral characteristics confirm the successful fabrication of uniformly disordered synbiotic nanoparticles and are widely accepted as indicators of amorphous nanosystems in current nanomedicine and functional food research.

The FTIR spectrum of I.BNPs demonstrates the formation of a stable protein–polysaccharide nano-based formulation (Fig. 4). The broad band near 3269 cm^{-1} signifies enhanced O–H and N–H stretching vibrations, indicative of extensive hydrogen bonding between inulin and BNPs, consistent with recent reports of polysaccharide–protein interactions in nanomaterials.[61,62] The persistence of amide I (1632 cm^{-1}) and amide II (1531 cm^{-1}) peaks confirm the preservation of BSA's secondary structure post-functionalization, vital for maintaining its bioactivity. Additional absorptions at 1229 cm^{-1} and 1379 cm^{-1} correspond to inulin's C–O and C–H stretching modes, verifying its successful incorporation into the nanoparticle matrix. Additionally, the polysaccharide nature of inulin (SI Fig 7) is being retained in the I.BNPs and our investigation revealed characteristic bands consistent with those reported for inulin by Akram and Garud in 2020.[63] The observed peak broadening and shifts compared to uncoated BNPs reflect increased molecular disorder and stronger hydrogen bonding, characteristic features of amorphous protein–polysaccharide composites reported in current FTIR analyses.[61,64]

4 Conclusion

This study successfully developed and characterized a nano-based synbiotic formulation (I.BNPs) as an efficient delivery platform for *Lactiplantibacillus plantarum* RJ2. Comprehensive physicochemical and structural analyses confirmed the formation of highly stable BSA nanostructures with superior homogeneity and electrostatic stability. Various structural characteristic methods demonstrated their nanoscale self-assembled morphology distinct from bulk and confirmed its improved stability. Protein estimation of the nanoparticle by the Lowry method verified the retention of BSA's protein nature and quantitative linearity across concentrations, confirming accurate nanoparticle formulation. The BNP-based synbiotic formulation was developed using *Lactiplantibacillus plantarum* RJ 2 and I.BNPs utilizing the sequential deposition technique. Functionally, the I.BNPs significantly enhanced probiotic performance,

achieving 95% survival under simulated gastrointestinal and acidic conditions and improved bile salt tolerance. The inulin coating conferred dual prebiotic and protective functions, minimizing cell damage and sustaining viability under stress.

Moreover, the sequentially engineered I.BNPs exhibited enhanced auto-aggregation and co-aggregation abilities, contributing to intestinal adhesion and pathogen exclusion, while antimicrobial susceptibility tests confirmed the retention of intrinsic, non-transferable antibiotic resistance. These findings establish the inulin-BSA platform as a biocompatible, stable, and functionally efficient nano-based synbiotic system capable of delivering probiotics with high viability, offering strong potential for application in nutraceutical, food, and therapeutic formulations.

Future research should hinge on *in vivo* validation with gastrointestinal transit models to demonstrate intestinal uptake and colonization of encapsulated probiotics. Detailed molecular research using advanced spectroscopic techniques such as Raman spectroscopy and solid-state NMR may help to better understand the interfacial interactions between inulin, BSA, and probiotic bacteria that contribute to the stability of nanosynbiotics. Furthermore, process improvement using scalable continuous flow desolvation systems would make good manufacturing practice (GMP) based production more efficient. Further research should focus on incorporating these nanosynbiotics into functional food matrices like vegan food products, fortified yogurt *etc.* while ensuring prolonged shelf-life stability and probiotic viability. In addition, phase I clinical safety studies will be required to validate its translational potential in probiotic administration systems.

Conflicts of interest

The authors confirm that there are no known conflicts of interest associated with this publication, and there has been no significant financial support for this work that could have influenced its outcome.

Data availability

All data generated or analyzed during this study are included in this published article and its supplementary information (SI), which contain the data supporting the findings reported herein. Supplementary information: Fig. 1: UV-visible absorption characteristics of BSA and BNPs. Fig. 2: FT-IR spectra of BSA. Fig 3: XRD spectra of BSA. Fig. 4: The standard BSA calibration curve. Fig 5: Antibiotic resistance characteristics of *Lactiplantibacillus plantarum* RJ 2 (a) and I.BNPs (b) against various antibiotics. Fig 6: XRD spectra of inulin. Fig. 7: FT-IR spectra of inulin. Table. 1: Absorbance at 660 nm based on different concentrations. See DOI: https://doi.org/10.1039/d5fb00846h.

Acknowledgements

The authors thank the Department of Optoelectronics, University of Kerala, and CSIR – NIIST, for FESEM analysis, and the Department of Chemistry, University of Kerala, for zetapotential and DLS analysis. We thank CLIF, University of Kerala, for FTIR and XRD analysis.

References

1 J. Clapp, *Food*, 2020, 1984.
2 A. Latif, A. Shehzad, S. Niazi, A. Zahid, W. Ashraf, M. W. Iqbal, A. Rehman, T. Riaz, R. M. Aadil, I. M. Khan, F. Özogul, J. M. Rocha, T. Esatbeyoglu and S. A. Korma, Probiotics: mechanism of action, health benefits and their application in food industries, *Front. Microbiol.*, 2023, **14**, 1216674.
3 L. I. G. de Oliveira, A. R. R. de Araujo, T. C. Pimentel, V. Capozzi, T. K. Alves Bezerra and M. Magnani, Probiotics and Prebiotics in Foodborne Illness: Mechanisms, Applications, and Future Directions, *J. Food Prot.*, 2025, **88**, 100584.
4 M. Ismael, M. Huang and Q. Zhong, The Bacteriocins Produced by Lactic Acid Bacteria and the Promising Applications in Promoting Gastrointestinal Health, *Foods*, 2024, **13**, 3887.
5 B. Sarita, D. Samadhan, M. Z. Hassan and E. G. Kovaleva, A comprehensive review of probiotics and human health-current prospective and applications, *Front. Microbiol.*, 2025, **15**, 1487641.
6 S. Raghuwanshi, S. Misra, R. Sharma and P. S. Bisen, Probiotics: Nutritional Therapeutic Tool, *J. Probiotics Heal.*, 2018, **6**, 194.
7 S. Ali, M. Hamayun, M. Siraj, S. A. Khan, H.-Y. Kim and B. Lee, Recent advances in prebiotics: Classification, mechanisms, and health applications, *Futur. Foods*, 2025, **12**, 100680.
8 İ. M. Alptekin, F. P. Çakıroğlu, T. Reçber and E. Nemutlu, Inulin may prevent the high-fat diet induced-obesity *via* suppressing endocannabinoid system in the prefrontal cortex in Wistar rats, *Int. J. Food Sci. Nutr.*, 2024, **75**, 800–811.
9 L.-Y. Zhou, Y. Xie and Y. Li, Bifidobacterium infantis regulates the programmed cell death 1 pathway and immune response in mice with inflammatory bowel disease, *World J. Gastroenterol.*, 2022, **28**, 3164–3176.
10 B. O. Schroeder, G. M. H. Birchenough, M. Ståhlman, L. Arike, M. E. V. Johansson, G. C. Hansson and F. Bäckhed, *Bifidobacteria* or Fiber Protects against Diet-Induced Microbiota-Mediated Colonic Mucus Deterioration, *Cell Host Microbe*, 2018, **23**, 27–40e7.
11 A. C. Ouwehand, K. Tiihonen, H. Mäkivuokko and N. Rautonen, in *Functional Dairy Products*, Elsevier, 2007, pp. 195–213.
12 P. Parhi, S. Q. Liu and W. S. Choo, Synbiotics: Effects of prebiotics on the growth and viability of probiotics in food matrices, *Bioact. Carbohydrates Diet. Fibre*, 2024, **32**, 100462.
13 S. Palai, C. M. P. Derecho, S. S. Kesh, C. Egbuna and P. C. Onyeike, in *Functional Foods and Nutraceuticals*, Springer International Publishing, Cham, 2020, pp. 173–196.
14 P. M. Reque and A. Brandelli, Encapsulation of probiotics and nutraceuticals: Applications in functional food industry, *Trends Food Sci. Technol.*, 2021, **114**, 1–10.

15 H. Liu, M. Xie and S. Nie, Recent trends and applications of polysaccharides for microencapsulation of probiotics, *Food Front*, 2020, **1**, 45–59.
16 A. H. Hemlata, N. Murali, S. Roy, S. Betal, S. Kumar and S. Minocha, Engineered BSA nanoparticles: Synthesis, drug loading, and advanced characterization, *Biol. Methods Protoc.*, 2025, **10**, bpaf066.
17 M. S. Virk, M. A. Virk, M. Gul, M. Awais, Q. Liang, T. Tufail, M. Zhong, Y. Sun, A. Qayum, E. A. El-Salam, J.-N. Ekumah, A. Rehman, A. Rashid and X. Ren, Layer-by-layer concurrent encapsulation of probiotics and bioactive compounds with supplementation in intermediary layers: An establishing instrument for microbiome recharge, core safety, and targeted delivery, *Food Hydrocoll*, 2025, **161**, 110873.
18 A. C. Anselmo, K. J. McHugh, J. Webster, R. Langer and A. Jaklenec, Layer-by-Layer Encapsulation of Probiotics for Delivery to the Microbiome, *Adv. Mater.*, 2016, **28**, 9486–9490.
19 M. Wang, J. Yang, M. Li, Y. Wang, H. Wu, L. Xiong and Q. Sun, Enhanced viability of layer-by-layer encapsulated *Lactobacillus pentosus* using chitosan and sodium phytate, *Food Chem.*, 2019, **285**, 260–265.
20 B. Liu, J. Hu, H. Yao, L. Zhang and H. Liu, Improved viability of probiotics encapsulated by layer-by-layer assembly using zein nanoparticles and pectin, *Food Hydrocoll.*, 2023, **143**, 108899.
21 E. Bronze-Uhle, B. C. Costa, V. F. Ximenes and P. N. Lisboa-Filho, Synthetic nanoparticles of bovine serum albumin with entrapped salicylic acid, *Nanotechnol. Sci. Appl.*, 2016, **10**, 11–21.
22 R. Rajam and C. Anandharamakrishnan, Microencapsulation of *Lactobacillus plantarum* (MTCC 5422) with fructooligosaccharide as wall material by spray drying, *LWT–Food Sci. Technol.*, 2015, **60**, 773–780.
23 Z. Fang, Z. Hongfei, Z. Junyu, P. Dziugan, L. Shanshan and Z. Bolin, Evaluation of probiotic properties of *Lactobacillus* strains isolated from traditional Chinese cheese, *Ann. Microbiol.*, 2015, **65**, 1419–1426.
24 Y. Nami, R. Vaseghi Bakhshayesh, H. Mohammadzadeh Jalaly, H. Lotfi, S. Eslami and M. A. Hejazi, Probiotic Properties of *Enterococcus* Isolated From Artisanal Dairy Products, *Front. Microbiol.*, 2019, **10**, 300.
25 M. Li, Y. Wang, H. Cui, Y. Li, Y. Sun and H.-J. Qiu, Characterization of Lactic Acid Bacteria Isolated From the Gastrointestinal Tract of a Wild Boar as Potential Probiotics, *Front. Vet. Sci.*, 2020, **7**, 49.
26 Y. Tanjung, M. Dewi, V. Gatera, M. Barliana, I. M. Joni and A. Chaerunisaa, Factors Affecting the Synthesis of Bovine Serum Albumin Nanoparticles Using the Desolvation Method, *Nanotechnol. Sci. Appl.*, 2024, **17**, 21–40.
27 J. A. Kramar, Dynamic light scattering distributions by any means, *J. Nanopart. Res.*, 2021, **23**, 120.
28 A. R. Karow, J. Götzl and P. Garidel, Resolving power of dynamic light scattering for protein and polystyrene nanoparticles, *Pharm. Dev. Technol.*, 2015, **20**, 84–89.
29 W. Alshaer, S. Alsotari, N. Aladaileh, A. Rifai, A. Khalaf, B. AlQuaissi, B. Sabbah, H. Nsairat and F. Odeh, Clarithromycin-Loaded Albumin-Based Nanoparticles for Improved Antibacterial and Anticancer Performance, *Pharmaceutics*, 2025, **17**, 729.
30 A. P. S. Tartari, S. H. Peczek, M. T. Fin, J. Ziebarth, C. S. Machado and R. M. Mainardes, Bovine Serum Albumin Nanoparticles Enhanced the Intranasal Bioavailability of Silybin in Rats, *Pharmaceutics*, 2023, **15**, 2648.
31 H. Kaur and A. Singh, Design, development and characterization of serratiopeptidase loaded albumin nanoparticles, *J. Appl. Pharm. Sci.*, 2015, 103–109.
32 F. Kiran, M. Afzaal, H. Shahid, F. Saeed, A. Ahmad, H. Ateeq, F. Islam, H. Yousaf, Y. A. Shah, G. A. Nayik, S. Alfarraj, M. J. Ansari and M. Asif Shah, Effect of protein-based nanoencapsulation on viability of probiotic bacteria under hostile conditions, *Int. J. Food Prop.*, 2023, **26**, 1698–1710.
33 A. Bhagwat, P. Bhushette and U. S. Annapure, Spray drying studies of probiotic *Enterococcus* strains encapsulated with whey protein and maltodextrin, *Beni-Suef Univ. J. Basic Appl. Sci.*, 2020, **9**, 33.
34 S. Sakoui, R. Derdak, O. L. Pop, D. C. Vodnar, B. Addoum, B.-E. Teleky, S. Elemer, A. Elmakssoudi, R. Suharoschi, A. Soukri and B. El Khalfi, Effect of encapsulated probiotic in Inulin-Maltodextrin-Sodium alginate matrix on the viability of *Enterococcus mundtii* SRBG1 and the rheological parameters of fermented milk, *Curr. Res. Food Sci.*, 2022, **5**, 1713–1719.
35 Y. Huang, Q. Guan, Y. Wu, C. Zheng, L. Zhong, W. Xie, J. Chen, J. Huang, Q. Wang and Y. Zheng, Microencapsulation of *Lactiplantibacillus plantarum* BXM2 in Bamboo Shoot-Derived Nanocellulose Hydrogel to Enhance Its Survivability, *Gels*, 2025, **11**, 465.
36 W.-G. Xin, Y.-H. Jiang, Y.-T. Zhao, M. Liang, X.-Y. Chen, S.-J. Liu and H.-Y. Suo, Encapsulation of *Lactiplantibacillus plantarum* in a sodium alginate/pectin/tea polyphenol complex: Enhancing stability and bioactivity for fermented milk products, *Food Chem.*, 2025, **488**, 144851.
37 Z. Dong, S. Yang, C. Tang, D. Li, Y. Kan and L. Yao, New insights into microbial bile salt hydrolases: from physiological roles to potential applications, *Front. Microbiol.*, 2025, **16**, 1513541.
38 W. Sheng, G. Ji and L. Zhang, Immunomodulatory effects of inulin and its intestinal metabolites, *Front. Immunol.*, 2024, **14**, 1224092.
39 N. Tuerhong, L. Wang, J. Cui, D. Shataer, H. Yan, X. Dong, Z. Gao, M. Zhang, Y. Qin and J. Lu, Targeted Screening of *Lactiplantibacillus plantarum* Strains Isolated from Tomatoes and Its Application in Tomato Fermented Juice, *Foods*, 2024, **13**, 3569.
40 R. Li and C. Bi, Comparative Genomic Analysis of *Lactiplantibacillus plantarum*: Insights into Its Genetic Diversity, Metabolic Function, and Antibiotic Resistance, *Genes*, 2025, **16**, 869.
41 A. V. Sarangarajan, A. Jain, J. L. Ferreir, Anushree, A. Dhanawat, P. Ahir and S. Acharya, The synbiotic solution: Evaluating safety and efficacy in antibiotic-associated dysbiosis - A randomized, double-blind,

placebo-controlled pre-clinical study with sprague dawley rats, *PharmaNutrition*, 2024, **29**, 100402.
42 A. Bhatia, D. Sharma, J. Mehta, V. Kumarasamy, M. Y. Begum, A. Siddiqua, M. Sekar, V. Subramaniyan, L. S. Wong and N. N. I. Mat Rani, Probiotics and Synbiotics: Applications, Benefits, and Mechanisms for the Improvement of Human and Ecological Health, *J. Multidiscip. Healthc.*, 2025, **18**, 1493–1510.
43 M. D'alessandro, C. Parolin, D. Bukvicki, L. Siroli, B. Vitali, M. De Angelis, R. Lanciotti and F. Patrignani, Probiotic and Metabolic Characterization of Vaginal *Lactobacilli* for a Potential Use in Functional Foods, *Microorganisms*, 2021, **9**, 833.
44 J. Isenring, A. Geirnaert, C. Lacroix and M. J. A. Stevens, Bistable auto-aggregation phenotype in *Lactiplantibacillus plantarum* emerges after cultivation in *in vitro* colonic microbiota, *BMC Microbiol*, 2021, **21**, 268.
45 A. Zawistowska-Rojek, A. Kośmider, K. Stępień and S. Tyski, Adhesion and aggregation properties of *Lactobacillaceae* strains as protection ways against enteropathogenic bacteria, *Arch. Microbiol.*, 2022, **204**, 285.
46 K. B. Klopper, S. M. Deane and L. M. T. Dicks, Aciduric Strains of *Lactobacillus reuteri* and *Lactobacillus rhamnosus*, Isolated from Human Feces, Have Strong Adhesion and Aggregation Properties, *Probiotics Antimicrob. Proteins*, 2018, **10**, 89–97.
47 B. Sophatha, S. Piwat and R. Teanpaisan, Adhesion, anti-adhesion and aggregation properties relating to surface charges of selected *Lactobacillus* strains: study in Caco-2 and H357 cells, *Arch. Microbiol.*, 2020, **202**, 1349–1357.
48 Y. Lei, Z. Xie, A. Zhao, J. P. Colarelli, M. J. Miller and Y. Lee, Layer-by-layer coating of *Lacticaseibacillus rhamnosus* GG (LGG) using chitosan and zein/tween-80/fucoidan nanoparticles to enhance LGG's survival under adverse conditions, *Food Hydrocoll.*, 2024, **154**, 110039.
49 S. Agriopoulou, S. Smaoui, M. Chaari, T. Varzakas, A. Can Karaca and S. M. Jafari, Encapsulation of Probiotics within Double/Multiple Layer Beads/Carriers: A Concise Review, *Molecules*, 2024, **29**, 2431.
50 Y.-Y. Zhu, R.-H. Ma, K. Thakur, W.-W. Zhang, J.-G. Zhang, M. R. Khan, C. Liao and Z.-J. Wei, Layer-by-layer nanoencapsulation strategies for enhanced oral delivery and function of *Lactobacillus plantarum* B2, *Food Hydrocoll.*, 2025, **160**, 110865.
51 L. Sánchez-segura, S. Zaina, A. F. Kú-gonzález, J. A. Guzmán-lópez, L. E. Zavala-garcía and M. G. López, Effect of Crosslinking Using Heat on the Physicochemical Features of Bsa – Capsaicin Nanoparticles, *Pharmaceutics*, 2025, **17**, 1306.
52 L. N. Hanh Cao, T. V. Nguyen, N. Q. Nguyen, T. B. Thuyen Nguyen, H. V. T. Luong and D. T. Pham, Alginate functionalized chitosan nanoparticles using multilayer co-axial electro-spraying for ovalbumin controlled release *via* oral delivery, *J. Drug Deliv. Sci. Technol.*, 2024, **96**, 105733.
53 C. Sardo, G. Auriemma, C. Mazzacano, C. Conte, V. Piccolo, T. Ciaglia, M. Denel-Bobrowska, A. B. Olejniczak, D. Fiore, M. C. Proto, P. Gazzerro and R. P. Aquino, Inulin Amphiphilic Copolymer-Based Drug Delivery: Unraveling the Structural Features of Graft Constructs, *Pharmaceutics*, 2024, **16**, 971.
54 W. S. Mota, P. Severino, V. Kadian, R. Rao, A. Zielińska, A. M. Silva, S. Mahant and E. B. Souto, Nanometrology: particle sizing and influence on the toxicological profile, *Front. Nanotechnol.*, 2025, **7**, 1479464.
55 A. Venugopal, D. Steinberg, O. Moyal, S. Yonassi, N. Glaicher, E. Gitelman, M. Shemesh and M. Amitay, Computational Analysis of Morphological Changes in *Lactiplantibacillus plantarum* Under Acidic Stress, *Microorganisms*, 2025, **13**, 647.
56 M. Wei, C. Han, X. Zhou, T. Tong, J. Zhang, X. Ji, P. Zhang, Y. Zhang, Y. Liu, X. Zhang, T. Cai and C. Xie, Filamentous morphology engineering of bacteria by iron metabolism modulation through MagR expression, *Synth. Syst. Biotechnol.*, 2024, **9**, 522–530.
57 Y. Wang, Y. Qu, X. Liu, J. Huang, C. Mao, C. Wang, S. Zhu, Y. Zheng, Z. Li, Z. Cui, H. Jiang, Y. Lv, J. Shen and S. Wu, Dual-functional probiotic hydrogel with puerarin integration for microbiota-neuroimmune regulation in antibiotic-free periodontitis therapy, *Bioact. Mater.*, 2025, **53**, 72–83.
58 A. Ohja, B. G. S, H. A. Pushpadass, M. E. E. Franklin, C. R. Grover, S. Kumar and A. Dhali, Encapsulation of *Lactiplantibacillus plantarum* CRD7 in sub-micron pullulan fibres by spray drying: Maximizing viability with prebiotic and thermal protectants, *Int. J. Biol. Macromol.*, 2024, **269**, 132068.
59 P. Zou, C. Costas, S. Jyakhwo, Y. Luo, L. Luo, Z. Wei and P. Otero, Hydrophilic composite nanoparticles of wheat gluten protein and carboxymethyl cellulose by pH cycle and its emulsification properties for loading curcumin, *Food Chem. X*, 2025, **31**, 103096.
60 H. Yang, S. Wang, L. Yang and H. Liu, Preparations, application of polysaccharide–protein nanoparticles and their assembly at the oil–water interface, *Food Sci. Biotechnol.*, 2024, **33**, 13–22.
61 M. Wang, S. Yang, N. Sun, T. Zhu, Z. Lian, S. Dai, J. Xu, X. Tong, H. Wang and L. Jiang, Soybean isolate protein complexes with different concentrations of inulin by ultrasound treatment: Structural and functional properties, *Ultrason. Sonochem.*, 2024, **105**, 106864.
62 S. Gholizadeh, A. Ehsani, S. Amjadi, H. Ahangari and V. Panahiazar, Green packaging system based on hybrid zein/inulin nanofibers activated with copper oxide nanoparticles and *Foeniculum vulgare* essential oil for preservation of fresh beef, *Appl. Food Res.*, 2025, **5**, 100724.
63 W. Akram and N. Garud, Optimization of inulin production process parameters using response surface methodology, *Future Journal of Pharmaceutical Sciences*, 2020, **6**, 68.
64 X. Zhao, D. Li, Y.-H. Lu, B. Rad, C. Yan, H. A. Bechtel, P. D. Ashby and M. B. Salmeron, In vitro investigation of protein assembly by combined microscopy and infrared spectroscopy at the nanometer scale, *Proc. Natl. Acad. Sci. U. S. A.*, 2022, **119**, e2200019119.

